

---

# AVA-VLA: IMPROVING VISION-LANGUAGE-ACTION MODELS WITH ACTIVE VISUAL ATTENTION

---

Lei Xiao<sup>1,\*</sup>, Jifeng Li<sup>1,\*</sup>, Juntao Gao<sup>1,2</sup>, Feiyang Ye<sup>1,†</sup>, Yan Jin<sup>1</sup>,  
 Jingjing Qian<sup>3</sup>, Jing Zhang<sup>2</sup>, Yong Wu<sup>1</sup>, Xiaoyuan Yu<sup>1,†</sup>

<sup>1</sup> LiAuto Inc.

<sup>2</sup> School of Information Science and Technology, Beijing University of Technology

<sup>3</sup> School of Data Science, The Chinese University of Hong Kong, Shenzhen

## ABSTRACT

Vision-Language-Action (VLA) models have demonstrated remarkable capabilities in embodied AI tasks. However, existing VLA models, often built upon Vision-Language Models (VLMs), typically process dense visual inputs independently at each timestep. This approach implicitly models the task as a Markov Decision Process (MDP). However, this history-agnostic design is suboptimal for effective visual token processing in dynamic sequential decision-making, as it fails to leverage the context of history. To address this limitation, we reformulate the problem from a Partially Observable Markov Decision Process (POMDP) perspective and propose a novel framework named AVA-VLA. Inspired by the POMDP that the action generation should be conditioned on the belief state. AVA-VLA introduces Active Visual Attention (AVA) to dynamically modulate visual processing. It achieves this by leveraging the recurrent state, which is a neural approximation of the agent’s belief state derived from the previous decision step. Specifically, the AVA module uses the recurrent state to compute the soft weights to actively process task-relevant visual tokens based on its historical context. Comprehensive evaluations demonstrate that AVA-VLA achieves state-of-the-art performance across popular robotic benchmarks, including LIBERO and CALVIN. Furthermore, real-world deployments on a dual-arm robot platform validate the framework’s practical applicability and robust sim-to-real transferability.

## 1 Introduction

Recent advances in robotic manipulation have demonstrated impressive progress in training robot action policies that can act across diverse real-world tasks. One transformative paradigm is Vision-Language-Action (VLA) models [4, 57, 2, 7, 17, 3, 32, 20], which integrate visual perception, natural language understanding, and action generation within a unified neural architecture. These models, capable of instruction following and robotic action generation, possess rich understanding capabilities and better generalization capabilities when fine-tuned for downstream scenarios.

To adopt the ability to understand diverse scenes, objects, and natural language instructions, most VLA models are built upon pretrained Vision-Language Models (VLMs) [26, 9, 16]. Such models typically extend VLM architectures by incorporating modules such as action tokenization [17, 39] or specialized action experts [51, 20] to enable action-oriented outputs. Based on this architectural inheritance, these VLA models typically process visual inputs as isolated temporal frames, treating each frame independently. This approach implicitly formulates the robot manipulation task as a Markov Decision Process (MDP) [28, 14], where actions are generated based on the current visual observation, as this observation is assumed to be the complete world state. In the context of realistic robotic manipulation, the current visual frame represents only a partial observation of the true state of the environment. This state encompasses non-observable dynamics that occur across temporal sequences, such as internal states and occluded information. By discarding the rich context available from the past, this MDP-based approach is suboptimal for the dynamic, sequential decision-making that lies in robotic manipulation tasks.

---

\*Equal contribution. † Corresponding author.

This limitation of the MDP-based assumption has significant impacts on VLA models, particularly for the model’s visual processing capabilities. The essence of VLA modeling is to construct a dynamic feedback control system, where the agent’s preceding action directly alters its current visual input. However, by processing frames in isolation, the visual attention weights, guided by the static language instruction, are forced to re-evaluate the independent visual information from scratch at each decision step. This lack of a global contextual understanding means the model cannot effectively filter out temporally redundant information and focus on visual regions that become essential given the past actions. This results in a visual system that is inactive rather than active. In fact, the inability to anticipate perceptual intent a priori makes it difficult to implement active visual modules in computer vision. The sequential dynamics inherent in sequential decision-making problems, however, create an opportunity to realize active visual perception. Recognizing the limitations of processing frames in isolation, some recent methods [52, 22, 46] have begun to leverage historical information, such as frame comparison result and KV-cache reuse, for efficient visual token processing [8, 54]. However, these approaches mainly focus on visual token pruning with the goal of improving model efficiency. Therefore, designing a more dynamic, context-aware visual processing paradigm to achieve more effective visual token processing that enhances VLA generalization quality remains a significant challenge.

To address this challenge, inspired by the theoretical framework of Partially Observable Markov Decision Process (POMDP) [38, 19], we propose the AVA-VLA framework. We remind that the core challenge identified above is similar to the POMDP challenge of forming a robust belief state, which functions as a summary of past observations and actions to guide decision-making under uncertainty. Since directly computing or representing the belief state is generally intractable, we introduce a recurrent state, which functions as a neural approximation of this belief state and is calculated by the intermediate output of the model in the previous time step. Then, we design an Active Visual Attention (AVA) module to leverage this recurrent state to calculating the importance of vision tokens and dynamically modulating the visual processing of the current frame. This allows the model to filter and focus its attention based on its historical belief, rather than purely static language instruction. Therefore, the proposed AVA-VLA framework does not rely solely on the current observation but learns to explicitly condition the action prediction on the recurrent state.

Through extensive experiments in both simulation benchmarks [25, 11, 28] and real-world tasks [5], we demonstrate that our proposed active visual attention module helps to improve policy performance compared to previous VLA frameworks. Our contributions are threefold:

- We propose the novel AVA-VLA framework to solve the critical limitation of lacking historical context in MDP-based VLA models. To our knowledge, it is the first VLA framework to explicitly address this limitation via a POMDP-inspired approach.
- We introduce an Active Visual Attention (AVA) module that leverages the recurrent state to dynamically modulate the visual processing of the current frame for action prediction.
- We conduct comprehensive evaluations in both simulation and the real-world tasks, demonstrating that AVA-VLA framework improves VLA performance, and our method achieves state-of-the-art performance across multiple robot tasks.

## 2 Related Work

**Vision-Language-Action Models.** VLMs [26, 9, 16, 37] have been pivotal in advancing robotic control by providing rich multi-modal representations. This has fostered the development of VLA models [4, 57, 2, 7, 17, 3, 32, 20] that bridge high-level perception with low-level action generation. A significant paradigm shift was the introduction of action tokenization by the RT series [4, 57, 1]. This approach treats control as a sequence modeling problem, enabling scalable

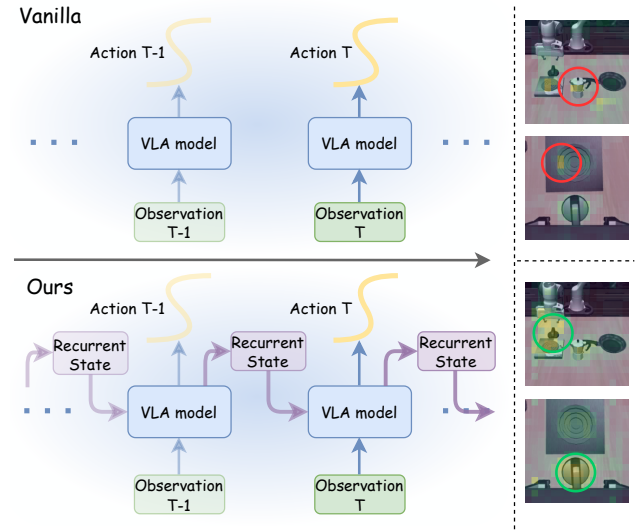


Figure 1: (a) Graphical models of the proposed AVA-VLA framework and vanilla VLAs. (b) The corresponding visualization of two viewpoints in executing “turn on the stove and put the moka pot on it”, where the vanilla OpenVLA-OFT [18] fails to locate “stove” switch according the time sequence.

web-to-robot transfer. Models like OpenVLA [17] and UniVLA [5] generate action policies in the autoregressive (AR) manner. While expressive, the sequential nature of AR decoding is computationally intensive. Therefore, recent research has diversified into more efficient and effective action decoding strategies. Models such as CogACT [20] and the  $\pi$  series [3, 32], have explored diffusion-based decoders for the iterative refinement of continuous action trajectories. Other recent works, such as OpenVLA-OFT [18] and its variant [21], employ parallel decoding, which enables the simultaneous prediction of actions within the action chunk, improving inference efficiency and supporting scalable deployment.

**Sequential Processing in VLMs.** Many VLM [33, 29, 47, 10] researches focus on processing sequential visual data for tasks such as video understanding and temporal-based video questions. These works efficiently aggregate historical information, allowing the model to build a holistic, temporal-aware representation of the video's content. VLM-3R [10] employs a geometry encoder to derive implicit 3D tokens that represent spatial-temporal understanding. [47] incrementally updates a persistent internal state that encodes the scene content. These VLM models use history for passive comprehension or offline understanding. In contrast, VLA models operate in an active, dynamic decision-making environment, which demands models to interact. This distinction motivates our POMDP-inspired approach, which focuses on maintaining a recurrent state for active decision-making.

### 3 Methods

In this section, we present our proposed VLA method. We begin with the preliminaries (3.1), followed by the AVA-VLA framework (3.2) and the detailed description of the proposed active visual attention module (3.3). We then explain our training and inference procedures (3.4).

#### 3.1 Preliminaries

A typical VLA model  $\mathcal{P}_\theta$ , parameterized by  $\theta$ , consists of four main components: a Large-Language-Model (LLM) backbone  $\mathcal{M}$ , a vision encoder  $\mathcal{E}$ , a language tokenizer  $\mathcal{T}$ , and an action head (or de-tokenizer)  $\mathcal{Q}$ . We thus define the model as  $\mathcal{P} = \{\mathcal{M}, \mathcal{E}, \mathcal{T}, \mathcal{Q}\}$ .

Following the representative OpenVLA [17], at timestep  $t$ , given an input tuple  $\mathbf{x}^t = (\mathbf{x}_I^t, \mathbf{x}_S^t)$ , the visual encoder  $\mathcal{E}$  first encodes the input image  $\mathbf{x}_I^t$  into  $L_I$  visual tokens:  $\mathbf{z}_I^t = \mathcal{E}(\mathbf{x}_I^t) \in \mathbb{R}^{L_I \times d}$ , where  $d$  denotes the embedding dimension. These visual tokens are then concatenated with  $L_S^t$  language tokens,  $\mathbf{z}_S^t = \mathcal{T}(\mathbf{x}_S^t) \in \mathbb{R}^{L_S^t \times d}$ . The combined sequence is then fed into the LLM backbone  $\mathcal{M}$  to generate output hidden states  $\mathbf{h}^t$ . Finally, the action head  $\mathcal{Q}$  maps the hidden states  $\mathbf{h}^t$  into a  $D$ -dimensional executable action  $\mathcal{A}^t$  for robotic control (e.g.,  $D = 7$  for 3-DoF translation, 3-DoF rotation, and binary gripper control). Thus, the entire forward pass at timestep  $t$  can be formulated as:

$$\mathcal{A}^t = \mathcal{Q}(\mathbf{h}^t) = \mathcal{Q}(\mathcal{M}(\mathbf{z}_I^t, \mathbf{z}_S^t)). \quad (1)$$

Recent representative VLA models, such as OpenVLA-OFT [18] and its variant [21], map the output hidden states into an executable action chunk  $\mathcal{A}^t = [a_0^t, a_1^t, \dots, a_{L_c-1}^t] \in \mathbb{R}^{L_c \times D}$ , where  $L_c$  and  $D$  represent the length of the action chunk and the dimensionality of each atomic action, respectively. To facilitate parallel generation, a learnable action placeholder embedding  $\mathbf{p}^t$  is appended to the input sequence [21, 24]. This placeholder embedding is set to empty in OpenVLA-OFT, i.e.,  $\mathbf{p}^t = \mathbf{0} = [\mathbf{0}_0, \mathbf{0}_1, \dots, \mathbf{0}_{L_c-1}] \in \mathbb{R}^{L_c \times D \times d}$ .

The corresponding forward pass under parallel decoding at timestep  $t$  can thus be expressed as:

$$\mathcal{A}^t = \mathcal{Q}(\mathcal{M}_{\text{parallel}}(\mathbf{z}_I^t, \mathbf{z}_S^t, \mathbf{p}^t)). \quad (2)$$

Regardless of whether AR or parallel decoding is used, these VLA models learn to predict the action  $\bar{\mathcal{A}}^t$  only from the current observation  $\mathbf{x}^t$ . This implicitly models the task as a Markov decision process:

$$\bar{\mathcal{A}}^t \sim \mathcal{P}_\theta(\mathcal{A}^t \mid \mathbf{x}^t). \quad (3)$$

#### 3.2 AVA-VLA Framework

The history-agnostic design for policy learning in Eq. (3) is suboptimal for effective visual token processing in dynamic sequential decision-making [53, 19], as it fails to capture non-observable dynamics or occluded information. This limitation inspired us to re-formulate the VLA model from a POMDP perspective. In a POMDP framework, the optimal policy at timestep  $t$  should be conditioned not only on the current observation  $\mathbf{x}^t$  but also on a belief state  $b^{t-1}$ , which

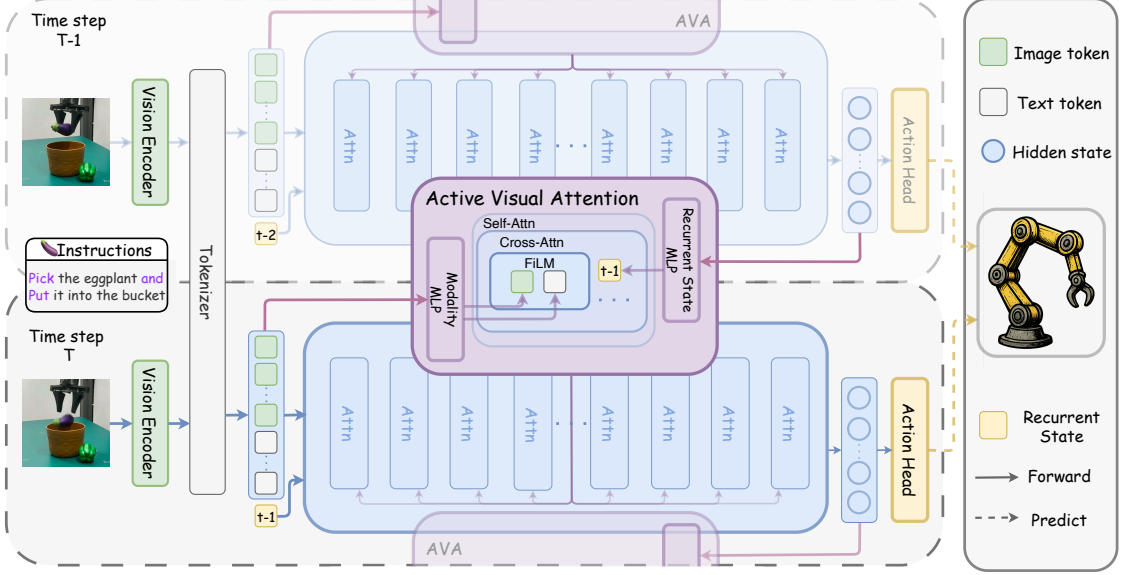


Figure 2: Overview of the proposed AVA-VLA framework.

captures all relevant historical context, including observations and actions, i.e.,  $b^{t-1} = P(s_{t-1} | \mathbf{x}^{<t}, \mathcal{A}^{<t})$ . Inspired by this theoretical framework, we re-formulate the VLA policy as

$$\bar{\mathcal{A}}^t \sim \mathcal{P}_\theta(\mathcal{A}^t | \mathbf{x}^t, b^{t-1}). \quad (4)$$

This formulation provides a theoretical foundation for designing a more effective visual processing paradigm, where lies an implication of leveraging historical context in observation can help to enhance VLA generalization. Since computing the theoretical belief state  $b^{t-1}$  is generally intractable, we instead propose to learn a compressed representation,  $r^{t-1}$ , as its neural approximation. This approach naturally transforms the VLA model into a recurrent structure [27], leading to a non-Markovian policy conditioned on this learned representation:  $\mathcal{A}^t \sim \mathcal{P}_\theta(\mathcal{A}^t | \mathbf{x}^t, r^{t-1})$ .

In our proposed AVA-VLA framework, we term this approximate vector  $r^{t-1}$  the recurrent state, which captures historical context. In typical VLA models, the hidden states immediately preceding action generation contain fused visual and language information and are predictive of the agent’s intent. Therefore, we derive the recurrent state for timestep  $t$  from the action-related hidden state at timestep  $t-1$ .

Specifically, for a parallel-decoding-based VLA model, which contains  $M$  decoder layers that predict  $\mathbf{L}_A = \mathbf{L}_c D$  actions in one forward pass, we denote its hidden states output at the  $m$ -th layer and time  $t$  by  $h_m^t \in \mathbb{R}^{\mathbf{L}_A \times d}$ . The corresponding recurrent state is computed by:

$$r^{t-1} = \mathcal{B}(h_M^{t-1}) \in \mathbb{R}^{\mathbf{L}_A \times d}, \quad (5)$$

where  $\mathcal{B}$  is an MLP module that transforms the hidden state into the recurrent state.

We employ this recurrent state to guide the VLA model to actively focus on visual regions that become critical along the time sequence. To utilize the recurrent state, we introduce the active visual attention module by quantifying the importance of vision tokens and dynamically modulating the processing of the visual frame for the current timestep. Moreover, in order to preserve the rich historical information, we use this recurrent state  $r^{t-1}$  for action placeholder [18, 21] embedding initialization, i.e.,  $\mathbf{p}^t = r^{t-1}$ .

For the simplicity of implementation, our framework builds upon the OpenVLA-OFT foundation model. Therefore, the corresponding forward pass at timestep  $t$ , incorporating the AVA module and the state-based placeholder initialization, is formulated as:

$$\mathcal{A}^t = \mathcal{Q}(\mathcal{M}_{\text{parallel}}(\mathbf{z}_I^t, \mathcal{V}(\mathbf{X}^t, r^{t-1}), \mathbf{z}_S^t, r^{t-1}), \quad (6)$$

where  $\mathcal{V}$  is the proposed AVA module, which takes the current observations and the recurrent state as input.

### 3.3 Active Visual Attention

We now describe the detailed architecture of the AVA module  $\mathcal{V}$ , which is designed to modulate visual processing in a dynamic manner.

The AVA module first employ the modality MLPs to encode the visual features  $\mathbf{z}_I^t$  and the instruction feature  $\mathbf{z}_S^t$  into  $\bar{\mathbf{z}}_I^t \in \mathbb{R}^{L_I \times d'}$  and  $\bar{\mathbf{z}}_S^t \in \mathbb{R}^{L_S \times d'}$ , respectively, where  $d' < d$ . A feature-wise linear modulation (FiLM) [31] is applied to condition the visual features on the language instruction, i.e.,  $\hat{\mathbf{z}}_I^t = \mathcal{F}_\gamma(\bar{\mathbf{z}}_S^t) \odot \bar{\mathbf{z}}_I^t + \mathcal{F}_\beta(\bar{\mathbf{z}}_S^t)$ . Then it uses the vision tokens  $\hat{\mathbf{z}}_I^t$  as the query,

$$\mathbf{Q}^t = W_Q \hat{\mathbf{z}}_I^t \in \mathbb{R}^{L_I \times d'}, \quad (7)$$

and the recurrent state as the key and value

$$\mathbf{K}^t, \mathbf{V}^t = (W_K / W_V) \hat{\mathbf{r}}^{t-1} \in \mathbb{R}^{L_A \times d'}, \quad (8)$$

where  $W_Q, W_K, W_V$  are linear projection layers, and  $\hat{\mathbf{r}}^{t-1} \in \mathbb{R}^{L_A \times d'}$  is the output of  $\mathbf{r}^{t-1}$  after MLP encoding. Then it computes the attention matrix and feeds the output into a self-attention layer

$$\mathbf{O}^t = \text{Self-Att}(\text{Cross-Att}(\mathbf{Q}^t, \mathbf{K}^t, \mathbf{V}^t)). \quad (9)$$

Inspired by [35, 41], we feed the resulting tokens  $\mathbf{O}^t \in \mathbb{R}^{L_I \times d'}$  into a Feedforward Neural Network (FFN), a linear layer  $\mathcal{W} : \mathbb{R}^{d'} \rightarrow \mathbb{R}^2$ , and apply a Softmax function along the feature dimension. This predicts the logits for enhancing or weakening each vision token as:

$$\rho^t = \text{Softmax}(\mathcal{W}(\text{FFN}(\mathbf{O}^t))) \in \mathbb{R}^{L_I \times 2}. \quad (10)$$

Then we compute the final soft weights for visual tokens at time  $t$  by  $\omega^t = \rho^t \gamma$ , where  $\gamma$  is a 2-dimensional vector. This soft weights directly represents the importance score of the visual tokens. The components of  $\gamma$ ,  $\gamma_0$  and  $\gamma_1$ , represent the scalar scores for enhancing and weakening a vision token, respectively.

The soft weights  $\omega^t$  is applied to all layers of the LLM backbone. Specifically, at time step  $t$ , let the total sequence length be  $L_o^t$ , we denote the attention score of the  $m$ -th layer by  $\mathbf{C}^{t,m} \in \mathbb{R}^{L_o^t \times L_o^t}$ , which is calculated by applying the original attention mask to the raw attention scores. The final attention matrix of the  $m$ -th layer  $\mathbf{A}^{t,m}$  is calculated by applying the soft attention mask matrix  $\mathbf{U}^t$  with the *Softmax* operation to  $\mathbf{C}^{t,m}$ :

$$\mathbf{A}_{i,j}^{t,m} = \frac{\exp(\mathbf{C}_{i,j}^{t,m}) \mathbf{U}_{i,j}^t}{\sum_{l=1}^{L_o^t} \exp(\mathbf{C}_{i,l}^{t,m}) \mathbf{U}_{i,l}^t}, \quad 1 \leq i, j \leq L_o^t, \quad (11)$$

where the soft attention matrix  $\mathbf{U}^t$  is constructed based on the soft weights vector  $\omega^t$ :

$$\mathbf{U}_{i,j}^t = \begin{cases} 1 & \text{if } i = j \text{ or } j \notin \Lambda_I, \quad 1 \leq i, j \leq L_o^t \\ \omega_j^t & \text{if } i \neq j \text{ and } j \in \Lambda_I, \quad 1 \leq i, j \leq L_o^t \end{cases}, \quad (12)$$

where the set  $\Lambda_I$  represents the vision tokens indices.

Therefore, the proposed AVA module uses the recurrent state and current visual observation to calculate soft weights to guide the VLA model to filter and focus its attention based on historical information. The overview of the proposed AVA-VLA framework is shown in Figure 2.

### 3.4 Training and Inference Procedure

The proposed AVA-VLA framework introduces a recurrent dependency through the recurrent state  $\mathbf{r}^{t-1}$ . Training such a recurrent model ideally requires backpropagation through time over the entire trajectory to capture long-term dependencies. However, given the substantial memory constraint and computational cost of modern VLA backbones, performing the full backpropagation through time is computationally prohibitive [30].

To address this challenge, we adopt a truncated backpropagation through time strategy [23]. We unroll the model for a fixed, short horizon. Specifically, for the  $n$ -th data in the training batch, it contains a continuous observation sequence  $\{\mathbf{x}^{t,n}\}_{t=0}^{T-1}$ . For each timestep  $t$  in this sequence, we calculate the action chunk prediction loss using the Mean Absolute Error (MAE):  $\mathcal{L}^{t,n} = \mathcal{L}(\mathcal{A}^{t,n}, \mathcal{A}_{\text{GT}}^{t,n})$ . To ensure the mean of the soft weight aligns with our expectation, we add an L2 penalty regularizer  $\mathcal{L}_\omega^{t,n}$  on the mean value of the weight vector  $\omega^{t,n}$ , defined as:

$$\mathcal{L}_\omega^{t,n} = \|\mu(\omega^{t,n}) - c\|, \quad (13)$$

where  $\mu(\cdot)$  is the mean function and  $c$  is a target mean hyperparameter. Therefore, the total loss of one training batch is the sum of the prediction loss and penalty loss of  $N$  truncated sequences:

$$\mathcal{L}_{\text{total}} = \sum_{n=1}^N \sum_{t=0}^{T-1} (\mathcal{L}^{t,n} + \lambda \mathcal{L}_\omega^{t,n}), \quad (14)$$

where  $N$  is the batch size, and  $\lambda$  is a balancing coefficient. In our experiments, we set  $T = 4$  to balance computational feasibility with the need to learn the temporal dynamics captured by the recurrent state. At the first timestep ( $t = 0$ ) of any sequence, the initial recurrent state  $\mathbf{r}^{-1}$  is initialized as a zero embedding, i.e.,  $\mathbf{r}^{-1} = \bar{\mathbf{0}}$ .

During inference, the model operates in a fully recurrent manner. At the beginning of a new episode ( $t = 0$ ), the initial recurrent state  $\mathbf{r}^{-1}$  is initialized as the zero embedding. Then, for each subsequent timestep  $t \geq 0$ , the agent receives the current observation  $\mathbf{x}^t$  and performs a single forward pass as defined in Eq. (6), conditioned on both  $\mathbf{x}^t$  and the previously computed recurrent state  $\mathbf{r}^{t-1}$ . This forward pass predicts the action chunk  $\mathcal{A}^t$  and simultaneously extracts the recurrent state  $\mathbf{r}^{t-1}$ . This loop continues for the entire inference process.

**Remark.** We explicitly note that the soft weights vector  $\omega^t$  computed by the AVA module has a natural application in vision token reduction [48, 22]. Vision tokens with low importance scores can be pruned to reduce the computational cost of the LLM backbone. While this is a valid direction for improving model efficiency, it is not the primary focus of this work. We provide a preliminary exploratory analysis on leveraging the weight vector to do token reduction, which further validates the effectiveness of our proposed method. Details can be found in Section 4.4.

## 4 Experiments

We evaluate the effectiveness of our approach through a set of experiments spanning both simulation benchmarks and real-world robot manipulation tasks. Additionally, we conduct a comprehensive ablation study and analysis to validate the effectiveness of our approach. All experiments are conducted on Nvidia A800 GPUs.

### 4.1 Experimental Setup

We conduct experiments on three challenging settings: the LIBERO [25] and CALVIN [28] benchmarks for evaluation in simulation environments, and a real-world table-mounted Mobile ALOHA robot with four test tasks, to validate the sim-to-real transferability and practical applicability of our method. We use the open-sourced OpenVLA-OFT [18] as our foundation model, which consists of a two-branch vision encoder (DINOv2 and SigLIP) and a LLaMA2-7B backbone [45]. *The implementation details are put in Appendix A.*

**LIBERO.** LIBERO [25] is a benchmark for lifelong robot learning. It uses a Franka Emika Panda arm in MuJoCo, with datasets split into four suites: LIBERO-Spatial, LIBERO-Object, LIBERO-Goal, and LIBERO-Long. It contains 5,000 episodes across 100 tasks. Data includes RGB images, proprioceptive states, and delta actions, with procedural generation for diversity. *LIBERO+ [11] is a challenging LIBERO-based benchmark, which offers a robust benchmarking framework with 7 perturbation dimensions and 21 sub-dimensions. It allows users to assess model performance across various challenges systematically. We conduct additional experiments on the LIBERO+ benchmark, and the results are put in Appendix C.*

**CALVIN.** CALVIN [28] is a simulated benchmark for language-conditioned, long-horizon manipulation, using a Franka Panda arm with RGBD observations, proprioception, and natural language goals. It evaluates sequential reasoning in VLA. CALVIN spans 34 tasks across four environments (A-D), with 20,000+ episodes, emphasizing unseen object generalization and multi-stage sequences (e.g., “open drawer, pick blue block, push into drawer”). Following [5], we used the CALVIN “ABC→D” setting, which means training on environments A, B, and C and evaluating on environment D, to evaluate performance on the zero-shot generalization tasks.

**Mobile ALOHA Real-Robot Experiments.** We use a stationary cobot magic dual-arm robot to assess our model’s adaptability to novel real-world environments with a small number of robot demonstrations. Following [5, 55], we perform evaluations across four challenging tasks. These include Pick and Place, which involves placing the bucket in the center, and then placing irregular-shaped objects into the bucket (e.g., “put <obj> into bucket”), and Sequenced Instruction Understanding, which requires executing multi-step commands like stacking a Tower of Hanoi (“Stack tower of hanoi”). We also test Flexible Object Folding, a deformable object manipulation task requiring a specific three-stage process to fold a towel (“fold towel twice”), and Dexterous Action, which involves fine-motor skills such as using a shovel to scoop small items (e.g., corn, sesame seeds) into a bowl. For each task, the dataset contains between 30 and 450 demonstrations. *The task suits details are put in Appendix B.*

### 4.2 Evaluations Results

**Baselines.** We selected recently published works as baselines. They are TraceVLA [56], WorldVLA [6],  $\pi_0$  [3],  $\pi_0$ -FAST [32], UnifiedVLA [50], OpenVLA-OFT [18], OpenVLA [17], SpatialVLA [34], CoT-VLA [55], NORA [13], PD-VLA [39], UniVLA [5], OpenVLA-OFT [18], FLOWER [36], VLA-Adapter [49], RIPT-VLA [42], Seer [44]. The results of these baselines in LIBERO and CALVIN benchmarks are based on original references or other published

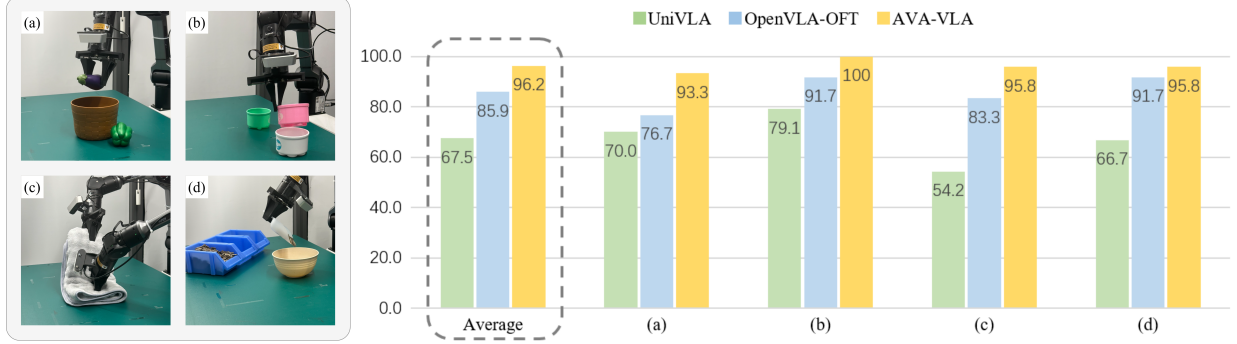


Figure 3: Comparison on the Mobile ALOHA real-robot experiments. Evaluation across four manipulation tasks, including (a) Pick and Place, (b) Sequenced Instruction Understanding, (c) Flexible Object Folding, (d) Dexterous Action. Left: Representative middle states for each task setup. Right: Task-specific success rates and cross-task averages for our method and baselines.

works, ensuring objectivity and correctness. The results of OpenVLA-OFT on the CALVIN benchmark were obtained using the official code, trained for 150,000 gradient steps with a batch size of 64. For Mobile ALOHA real-robot experiments, we select UniVLA and OpenVLA-OFT methods as baselines.

**Evaluation Metrics.** We use widely used performance evaluation metrics “Success Rate (SR)” (the same in LIBERO [25]) to evaluate the results for three challenging settings. In addition, we use “Average len” of completed tasks (the larger the better, with values between 0-5) as metrics for the CALVIN benchmark.

Table 1: Comparison on the LIBERO benchmark. The results are reported in two groups: one policy for all 4 suites, and one policy per suite. The best results in each column of each group are highlighted in **bold**.

Method	Spatial SR (%)	Object SR (%)	Goal SR (%)	Long SR (%)	Average SR (%)
<i>One policy for all 4 suites</i>					
TraceVLA [56]	84.6	85.2	75.1	54.1	74.8
WorldVLA [6]	87.6	96.2	83.4	60.0	81.8
$\pi_0$ [3]	96.8	98.8	95.8	85.2	94.2
$\pi_0$ -FAST [32]	96.4	96.8	88.6	60.2	85.5
UnifiedVLA [50]	95.4	98.8	93.6	94.0	95.5
OpenVLA-OFT [18]	<b>97.7</b>	98.0	96.1	95.3	96.8
AVA-VLA (Ours)	97.4	<b>99.4</b>	<b>97.4</b>	<b>97.6</b>	<b>98.0</b>
<i>One policy per suite</i>					
OpenVLA [17]	84.7	88.4	79.2	53.7	76.5
SpatialVLA [34]	88.2	89.9	78.6	55.5	78.1
CoT-VLA [55]	87.5	91.6	87.6	69.0	83.9
NORA [13]	92.2	95.4	89.4	74.6	87.9
PD-VLA [39]	95.5	96.7	94.9	91.7	94.7
UniVLA [5]	96.5	96.8	95.6	92.0	95.2
OpenVLA-OFT [18]	97.6	98.4	97.9	94.5	97.1
FLOWER [36]	97.5	99.1	96.1	94.9	96.9
VLA-Adapter [49]	97.8	99.2	97.2	95.0	97.3
RIPT-VLA [42]	99.0	98.6	<b>98.6</b>	93.8	97.5
AVA-VLA (Ours)	<b>99.2</b>	<b>99.6</b>	98.2	<b>96.2</b>	<b>98.3</b>

**LIBERO.** We present quantitative results in Table 1. Following established baselines, we conduct experiments in two different settings: training policies on each task suite independently (single-task learning) and training a single policy for all task suites (multi-task learning). Results demonstrate that the proposed AVA-VLA framework achieves state-of-the-art overall performance in both single-task and multi-task settings. Moreover, it consistently achieves the best performance on the most challenging LIBERO-Long task suite. These results demonstrate the superiority of the proposed AVA-VLA framework.

**CALVIN.** We present the success rates for each task and the average completed length across all five tasks of the CALVIN benchmark in Table 2. The results show that the proposed AVA-VLA framework comprehensively outperforms

Table 2: Comparison on the CALVIN ABC→D benchmark in terms of success rates (%) and average length. The best results in each column are highlighted in **bold**.

CALVIN ABC→D	Task completed in a row ↑					Avg. len ↑
	1	2	3	4	5	
OpenVLA [17]	91.3	77.8	62.0	52.1	43.5	3.27
UniVLA [5]	95.5	85.8	75.4	66.9	56.5	3.80
UnifiedVLA [50]	98.9	94.8	89.0	82.8	75.1	4.41
OpenVLA-OFT [18]	96.9	92.0	85.7	80.4	72.9	4.28
FLOWER [36]	99.4	95.8	90.7	84.9	77.8	4.53
VLA-Adapter [49]	99.1	94.6	88.8	82.8	76.5	4.42
Seer [44]	96.3	91.6	86.1	80.3	74.0	4.28
AVA-VLA (Ours)	<b>99.6</b>	<b>97.6</b>	<b>94.1</b>	<b>89.9</b>	<b>84.1</b>	<b>4.65</b>

baseline methods across all tasks. This demonstrates our method’s strong generalization ability, with an average length superior to previous state-of-the-art baselines.

**Mobile ALOHA.** The Pick and Place task is evaluated for a total of 30 trials (10 per object), while other tasks are evaluated for 24 trials each. The experimental results on real-world tasks are reported in Figure 3. In this setting, models are fine-tuned on a relatively small set of demonstrations. The results demonstrate that the proposed model possesses robust semantic understanding and dexterous action capabilities after training. Overall, AVA-VLA achieves the highest average performance compared to baseline approaches, confirming its sim-to-real transferability and practical applicability. We provide the execution trajectories of the four real-world task suites in Figure 4. The proposed AVA-VLA method can perform various tasks in real-world scenarios.

### 4.3 Ablation Studies

**Model Backbones.** To validate the effectiveness of the proposed framework, following [49], we compare three kinds of backbones: The OpenVLA-7B backbone [17] pre-trained on robotic data, the prismatic VLM trained on LLaMA2-7B [45], and the prismatic VLM [16] trained on Qwen2.5-0.5B [43]. The last two are different-scale backbones without pre-training on robotic data. We compare the proposed method against the standard OpenVLA-OFT method on the LIBERO-Long task suite in the single task setting. Results reported in Table 3 show that our method improves performance across different backbones, even on backbones not pre-trained on robotic datasets.

Table 3: Ablation study on the model backbones. Comparison on the LIBERO-Long task suite in the LIBERO benchmark in terms of success rates (%). The best results of each model backbone setting are highlighted in **bold**.

Backbones	OpenVLA-OFT	AVA-VLA
OpenVLA-7B [17]	94.5	<b>96.2</b> (1.7% ↑)
LLaMA2-7B [45]	90.0	<b>92.6</b> (2.6% ↑)
Qwen2.5-0.5B [43]	89.4	<b>90.8</b> (1.4% ↑)

**AVA module, and state-based initialization.** The AVA-VLA framework consists of two components: the AVA module and the state-based initialization strategy. To validate their individual effectiveness, we conduct ablation experiments on the LIBERO benchmark. These experiments use the “one policy for all 4 suites” setting, with results reported in Table 4. The results show that while both components improve performance over the OpenVLA-OFT baseline individually, neither matches the performance achieved by their combination. This demonstrates the effectiveness of both components grounded in the recurrent state.

### 4.4 Analysis

**Qualitative Visualization.** To understand the AVA module’s focus during task execution, we visualize the soft weights  $\omega^t$  with respect to the corresponding visual tokens during inference. Figure 5 displays results from two viewpoints. The visualization shows that the attention weights consistently focus on the robotic arm’s contact region and object positions. This demonstrates the module’s ability to actively capture important visual features, validating its effectiveness.

**Visual Token Reduction.** The proposed AVA module has a potential application in visual token reduction. Although visual token pruning causes the model to lose some visual information, it reduces the model’s computational cost and is beneficial for efficient inference [52, 50, 46, 15]. To validate that our AVA module effectively prioritizes task-relevant information, we apply a direct ranking strategy to prune visual tokens during inference. Specifically, for a given pruning



Figure 4: Visualization of proposed AVA-VLA's manipulation process on four long-horizon real-world tasks, showing key execution stage observations.

Table 4: Ablation study on the two main components in the AVA-VLA framework. The results on the LIBERO benchmark in terms of success rates (%) under the “one policy for all 4 suites” setting are reported. The best results in each column are highlighted in **bold**.

Method	Spatial SR (%)	Object SR (%)	Goal SR (%)	Long SR (%)	Average SR (%)
OpenVLA-OFT	97.7	98.0	96.1	95.3	96.8
AVA-VLA (State-based initialization)	97.2	98.8	96.6	97.2	97.5
AVA-VLA (AVA module)	<b>97.8</b>	98.6	97.0	96.6	97.5
AVA-VLA (AVA module + State-based initialization)	97.4	<b>99.4</b>	<b>97.4</b>	<b>97.6</b>	<b>98.0</b>

Table 5: Study on the visual token pruning with different pruning ratios. The results on the LIBERO benchmark in terms of success rates (%) under the “one policy for all 4 suites” setting are reported.

Pruning Ratio	Spatial SR (%)	Object SR (%)	Goal SR (%)	Long SR (%)	Avg. SR (%)
0%	97.4	99.4	97.4	97.6	98.0
50%	97.2	99.4	97.2	95.2	97.3
60%	97.6	99.4	97.0	95.0	97.3
70%	97.4	99.2	98.0	94.6	97.3
80%	96.8	98.2	96.2	92.8	96.0
90%	94.2	97.8	94.2	89.2	93.9

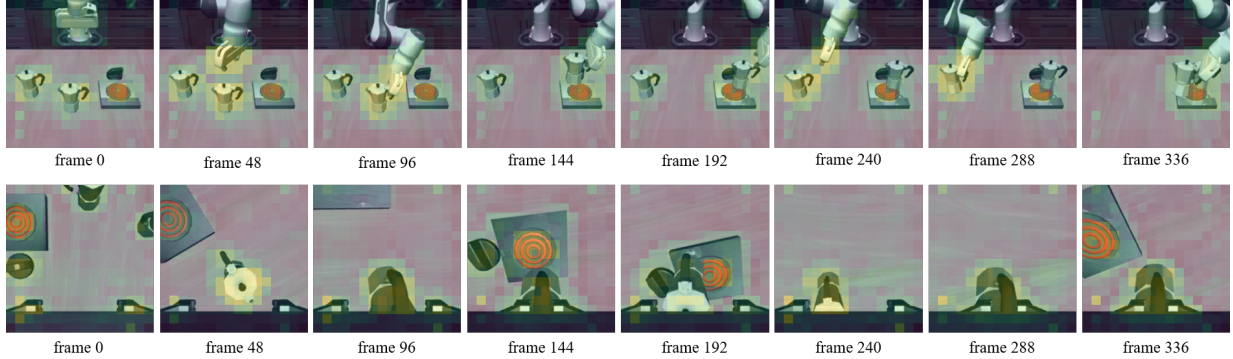


Figure 5: Visual dynamics of the soft weights during the task “put both moka pots on the stove” in two viewpoints.

ratio, we rank all visual tokens by their soft weights and retain only the top-ranked portion corresponding to the desired retention percentage. The results reported in Table 5, demonstrate the robustness of our method: the model suffers only a negligible performance decrease after pruning. Notably, with pruning ratios of 50%, 60%, and 70%, the proposed method continues to outperform the OpenVLA-OFT and maintains performance comparable to the state-of-the-art baselines reported in Table 1. The decline in success rate mainly comes from the most challenging LIBERO Long task suite, while the results remain consistent across other tasks suites. Even after reducing 90% of the visual tokens, our method still outperforms many baseline methods listed in Table 1. This result further demonstrates the effectiveness of the proposed AVA-VLA framework.

## 5 Conclusion

In this paper, we reformulate the robot manipulation problem from a POMDP perspective and propose a novel AVA-VLA framework. Unlike previous vision-language-action models that model the task as an MDP and process each frame independently, we introduce the recurrent state as a neural approximation of the agent’s belief state and design an Active Visual Attention (AVA) module that leverages this recurrent state to dynamically modulate the visual processing of the current frame. Our method enables the model to actively filter irrelevant information and focus on task-critical features based on its rich historical context. Extensive experiments demonstrate the superiority of the proposed AVA-VLA framework by achieving state-of-the-art performance across multiple robot simulation benchmarks, including LIBERO and CALVIN. It can also successfully transfer to diverse real-world robotic tasks, showing strong sim-to-real generalization.

## References

- [1] Suneel Belkhale, Tianli Ding, Ted Xiao, Pierre Sermanet, Quon Vuong, Jonathan Tompson, Yevgen Chebotar, Debidatta Dwibedi, and Dorsa Sadigh. Rt-h: Action hierarchies using language. *arXiv preprint arXiv:2403.01823*, 2024.
- [2] Johan Bjorck, Fernando Castañeda, Nikita Cherniadev, Xingye Da, Runyu Ding, Linxi Fan, Yu Fang, Dieter Fox, Fengyuan Hu, Spencer Huang, et al. Gr00t n1: An open foundation model for generalist humanoid robots. *arXiv preprint arXiv:2503.14734*, 2025.
- [3] Kevin Black, Noah Brown, Danny Driess, Adnan Esmail, Michael Equi, Chelsea Finn, Niccolò Fusai, Lachy Groom, Karol Hausman, Brian Ichter, et al.  $\pi_0$ : A vision-language-action flow model for general robot control. *arXiv preprint arXiv:2410.24164*, 2024.
- [4] Anthony Brohan, Noah Brown, Justice Carbajal, Yevgen Chebotar, Joseph Dabis, Chelsea Finn, Keerthana Gopalakrishnan, Karol Hausman, Alex Herzog, Jasmine Hsu, et al. Rt-1: Robotics transformer for real-world control at scale. *arXiv preprint arXiv:2212.06817*, 2022.
- [5] Qingwen Bu, Yanting Yang, Jisong Cai, Shenyuan Gao, Guanghui Ren, Maoqing Yao, Ping Luo, and Hongyang Li. Univla: Learning to act anywhere with task-centric latent actions. *arXiv preprint arXiv:2505.06111*, 2025.
- [6] Jun Cen, Chaohui Yu, Hangjie Yuan, Yuming Jiang, Siteng Huang, Jiayan Guo, Xin Li, Yibing Song, Hao Luo, Fan Wang, et al. Worldvla: Towards autoregressive action world model. *arXiv preprint arXiv:2506.21539*, 2025.
- [7] Chilam Cheang, Sijin Chen, Zhongren Cui, Yingdong Hu, Liqun Huang, Tao Kong, Hang Li, Yifeng Li, Yuxiao Liu, Xiao Ma, et al. Gr-3 technical report. *arXiv preprint arXiv:2507.15493*, 2025.
- [8] Liang Chen, Haozhe Zhao, Tianyu Liu, Shuai Bai, Junyang Lin, Chang Zhou, and Baobao Chang. An image is worth 1/2 tokens after layer 2: Plug-and-play inference acceleration for large vision-language models. In *European Conference on Computer Vision*, pp. 19–35. Springer, 2024.
- [9] Xi Chen, Xiao Wang, Lucas Beyer, Alexander Kolesnikov, Jialin Wu, Paul Voigtlaender, Basil Mustafa, Sebastian Goodman, Ibrahim Alabdulmohsin, Piotr Padlewski, et al. Pali-3 vision language models: Smaller, faster, stronger. *arXiv preprint arXiv:2310.09199*, 2023.
- [10] Zhiwen Fan, Jian Zhang, Renjie Li, Junge Zhang, Runjin Chen, Hezhen Hu, Kevin Wang, Huaizhi Qu, Dilin Wang, Zhicheng Yan, et al. Vlm-3r: Vision-language models augmented with instruction-aligned 3d reconstruction. *arXiv preprint arXiv:2505.20279*, 2025.
- [11] Senyu Fei, Siyin Wang, Junhao Shi, Zihao Dai, Jikun Cai, Pengfang Qian, Li Ji, Xinzhe He, Shiduo Zhang, Zhaoye Fei, et al. Libero-plus: In-depth robustness analysis of vision-language-action models. *arXiv preprint arXiv:2510.13626*, 2025.
- [12] Edward J Hu, Yelong Shen, Phillip Wallis, Zeyuan Allen-Zhu, Yuanzhi Li, Shean Wang, Lu Wang, Weizhu Chen, et al. Lora: Low-rank adaptation of large language models. *ICLR*, 1(2):3, 2022.
- [13] Chia-Yu Hung, Qi Sun, Pengfei Hong, Amir Zadeh, Chuan Li, U Tan, Navonil Majumder, Soujanya Poria, et al. Nora: A small open-sourced generalist vision language action model for embodied tasks. *arXiv preprint arXiv:2504.19854*, 2025.
- [14] Anqing Jiang, Yu Gao, Yiru Wang, Zhigang Sun, Shuo Wang, Yuwen Heng, Hao Sun, Shichen Tang, Lijuan Zhu, Jinhao Chai, et al. Irl-vla: Training an vision-language-action policy via reward world model. *arXiv preprint arXiv:2508.06571*, 2025a.
- [15] Titong Jiang, Xuefeng Jiang, Yuan Ma, Xin Wen, Bailin Li, Kun Zhan, Peng Jia, Yahui Liu, Sheng Sun, and Xianpeng Lang. The better you learn, the smarter you prune: Towards efficient vision-language-action models via differentiable token pruning. *arXiv preprint arXiv:2509.12594*, 2025b.
- [16] Siddharth Karamcheti, Suraj Nair, Ashwin Balakrishna, Percy Liang, Thomas Kollar, and Dorsa Sadigh. Prismatic vlms: Investigating the design space of visually-conditioned language models. In *Forty-first International Conference on Machine Learning*, 2024.
- [17] Moo Jin Kim, Karl Pertsch, Siddharth Karamcheti, Ted Xiao, Ashwin Balakrishna, Suraj Nair, Rafael Rafailov, Ethan Foster, Grace Lam, Pannag Sanketi, et al. Openvla: An open-source vision-language-action model. *arXiv preprint arXiv:2406.09246*, 2024.
- [18] Moo Jin Kim, Chelsea Finn, and Percy Liang. Fine-tuning vision-language-action models: Optimizing speed and success. *arXiv preprint arXiv:2502.19645*, 2025.
- [19] Mikko Lauri, David Hsu, and Joni Pajarinen. Partially observable markov decision processes in robotics: A survey. *IEEE Transactions on Robotics*, 39(1):21–40, 2022.

[20] Qixiu Li, Yaobo Liang, Zeyu Wang, Lin Luo, Xi Chen, Mozheng Liao, Fangyun Wei, Yu Deng, Sicheng Xu, Yizhong Zhang, et al. Cogact: A foundational vision-language-action model for synergizing cognition and action in robotic manipulation. *arXiv preprint arXiv:2411.19650*, 2024.

[21] Wei Li, Renshan Zhang, Rui Shao, Jie He, and Liqiang Nie. Cogvla: Cognition-aligned vision-language-action model via instruction-driven routing & sparsification. *arXiv preprint arXiv:2508.21046*, 2025a.

[22] Ye Li, Yuan Meng, Zewen Sun, Kangye Ji, Chen Tang, Jiajun Fan, Xinzhu Ma, Shutao Xia, Zhi Wang, and Wenwu Zhu. Sp-vla: A joint model scheduling and token pruning approach for vla model acceleration. *arXiv preprint arXiv:2506.12723*, 2025b.

[23] Renjie Liao, Yuwen Xiong, Ethan Fetaya, Lisa Zhang, KiJung Yoon, Xaq Pitkow, Raquel Urtasun, and Richard Zemel. Reviving and improving recurrent back-propagation. In *International conference on machine learning*, pp. 3082–3091. PMLR, 2018.

[24] Shengsheng Lin, Weiwei Lin, Wentai Wu, Songbo Wang, and Yongxiang Wang. Petformer: Long-term time series forecasting via placeholder-enhanced transformer. *IEEE Transactions on Emerging Topics in Computational Intelligence*, 2024.

[25] Bo Liu, Yifeng Zhu, Chongkai Gao, Yihao Feng, Qiang Liu, Yuke Zhu, and Peter Stone. Libero: Benchmarking knowledge transfer for lifelong robot learning. *Advances in Neural Information Processing Systems*, 36:44776–44791, 2023a.

[26] Haotian Liu, Chunyuan Li, Qingyang Wu, and Yong Jae Lee. Visual instruction tuning. *Advances in neural information processing systems*, 36:34892–34916, 2023b.

[27] Larry R Medsker, Lakhmi Jain, et al. Recurrent neural networks. *Design and applications*, 5(64-67):2, 2001.

[28] Oier Mees, Lukas Hermann, Erick Rosete-Beas, and Wolfram Burgard. Calvin: A benchmark for language-conditioned policy learning for long-horizon robot manipulation tasks. *IEEE Robotics and Automation Letters*, 7(3):7327–7334, 2022.

[29] Feiyu Pan, Hao Fang, Fangkai Li, Yanyu Xu, Yawei Li, Luca Benini, and Xiankai Lu. Semantic and sequential alignment for referring video object segmentation. In *Proceedings of the Computer Vision and Pattern Recognition Conference*, pp. 19067–19076, 2025.

[30] Razvan Pascanu, Tomas Mikolov, and Yoshua Bengio. On the difficulty of training recurrent neural networks. In *International conference on machine learning*, pp. 1310–1318. Pmlr, 2013.

[31] Ethan Perez, Florian Strub, Harm De Vries, Vincent Dumoulin, and Aaron Courville. Film: Visual reasoning with a general conditioning layer. In *Proceedings of the AAAI conference on artificial intelligence*, volume 32, 2018.

[32] Karl Pertsch, Kyle Stachowicz, Brian Ichter, Danny Driess, Suraj Nair, Quan Vuong, Oier Mees, Chelsea Finn, and Sergey Levine. Fast: Efficient action tokenization for vision-language-action models. *arXiv preprint arXiv:2501.09747*, 2025.

[33] Rui Qian, Xiaoyi Dong, Pan Zhang, Yuhang Zang, Shuangrui Ding, Dahua Lin, and Jiaqi Wang. Streaming long video understanding with large language models. *Advances in Neural Information Processing Systems*, 37:119336–119360, 2024.

[34] Delin Qu, Haoming Song, Qizhi Chen, Yuanqi Yao, Xinyi Ye, Yan Ding, Zhigang Wang, JiaYuan Gu, Bin Zhao, Dong Wang, et al. Spatialvla: Exploring spatial representations for visual-language-action model. *arXiv preprint arXiv:2501.15830*, 2025.

[35] Yongming Rao, Wenliang Zhao, Benlin Liu, Jiwen Lu, Jie Zhou, and Cho-Jui Hsieh. Dynamicvit: Efficient vision transformers with dynamic token sparsification. *Advances in neural information processing systems*, 34:13937–13949, 2021.

[36] Moritz Reuss, Hongyi Zhou, Marcel Röhle, Ömer Erdinç Yağmurlu, Fabian Otto, and Rudolf Lioutikov. Flower: Democratizing generalist robot policies with efficient vision-language-action flow policies. *arXiv preprint arXiv:2509.04996*, 2025.

[37] Leyang Shen, Gongwei Chen, Rui Shao, Weili Guan, and Liqiang Nie. Mome: Mixture of multimodal experts for generalist multimodal large language models. *Advances in neural information processing systems*, 37:42048–42070, 2024.

[38] Richard D Smallwood and Edward J Sondik. The optimal control of partially observable markov processes over a finite horizon. *Operations research*, 21(5):1071–1088, 1973.

[39] Wexuan Song, Jiayi Chen, Pengxiang Ding, Han Zhao, Wei Zhao, Zhide Zhong, Zongyuan Ge, Jun Ma, and Haoang Li. Accelerating vision-language-action model integrated with action chunking via parallel decoding. *arXiv preprint arXiv:2503.02310*, 2025.

[40] Wenxuan Song, Ziyang Zhou, Han Zhao, Jiayi Chen, Pengxiang Ding, Haodong Yan, Yuxin Huang, Feilong Tang, Donglin Wang, and Haoang Li. Reconvla: Reconstructive vision-language-action model as effective robot perceiver. *arXiv preprint arXiv:2508.10333*, 2025.

[41] Yizheng Sun, Yanze Xin, Hao Li, Jingyuan Sun, Chenghua Lin, and Riza Theresa Batista-Navarro. Lvpruning: An effective yet simple language-guided vision token pruning approach for multi-modal large language models. In *Findings of the Association for Computational Linguistics: NAACL 2025*, pp. 4299–4308, 2025.

[42] Shuhan Tan, Kairan Dou, Yue Zhao, and Philipp Krähenbühl. Interactive post-training for vision-language-action models. *arXiv preprint arXiv:2505.17016*, 2025.

[43] Qwen Team et al. Qwen2 technical report. *arXiv preprint arXiv:2407.10671*, 2(3), 2024.

[44] Yang Tian, Sizhe Yang, Jia Zeng, Ping Wang, Dahua Lin, Hao Dong, and Jiangmiao Pang. Predictive inverse dynamics models are scalable learners for robotic manipulation. *arXiv preprint arXiv:2412.15109*, 2024.

[45] Hugo Touvron, Louis Martin, Kevin Stone, Peter Albert, Amjad Almahairi, Yasmine Babaei, Nikolay Bashlykov, Soumya Batra, Prajjwal Bhargava, Shruti Bhosale, et al. Llama 2: Open foundation and fine-tuned chat models. *arXiv preprint arXiv:2307.09288*, 2023.

[46] Hanzhen Wang, Jiaming Xu, Jiayi Pan, Yongkang Zhou, and Guohao Dai. Specprune-vla: Accelerating vision-language-action models via action-aware self-speculative pruning. *arXiv preprint arXiv:2509.05614*, 2025a.

[47] Qianqian Wang, Yifei Zhang, Aleksander Holynski, Alexei A Efros, and Angjoo Kanazawa. Continuous 3d perception model with persistent state. In *Proceedings of the Computer Vision and Pattern Recognition Conference*, pp. 10510–10522, 2025b.

[48] Tiannan Wang, Wangchunshu Zhou, Yan Zeng, and Xinsong Zhang. Efficientvlm: Fast and accurate vision-language models via knowledge distillation and modal-adaptive pruning. In *Findings of the association for computational linguistics: ACL 2023*, pp. 13899–13913, 2023.

[49] Yihao Wang, Pengxiang Ding, Lingxiao Li, Can Cui, Zirui Ge, Xinyang Tong, Wenxuan Song, Han Zhao, Wei Zhao, Pengxu Hou, et al. Vla-adapter: An effective paradigm for tiny-scale vision-language-action model. *arXiv preprint arXiv:2509.09372*, 2025.

[50] Yuqi Wang, Xinghang Li, Wenxuan Wang, Junbo Zhang, Yingyan Li, Yuntao Chen, Xinlong Wang, and Zhaoxiang Zhang. Unified vision-language-action model. *arXiv preprint arXiv:2506.19850*, 2025c.

[51] Junjie Wen, Yichen Zhu, Jinning Li, Minjie Zhu, Zhibin Tang, Kun Wu, Zhiyuan Xu, Ning Liu, Ran Cheng, Chaomin Shen, et al. Tinyvla: Towards fast, data-efficient vision-language-action models for robotic manipulation. *IEEE Robotics and Automation Letters*, 2025.

[52] Siyu Xu, Yunke Wang, Chenghao Xia, Dihao Zhu, Tao Huang, and Chang Xu. Vla-cache: Towards efficient vision-language-action model via adaptive token caching in robotic manipulation. *arXiv preprint arXiv:2502.02175*, 2025.

[53] Shiqi Zhang, Piyush Khandelwal, and Peter Stone. Dynamically constructed (po) mdps for adaptive robot planning. In *Proceedings of the AAAI conference on artificial intelligence*, volume 31, 2017.

[54] Yuan Zhang, Chun-Kai Fan, Junpeng Ma, Wenzhao Zheng, Tao Huang, Kuan Cheng, Denis Gudovskiy, Tomoyuki Okuno, Yohei Nakata, Kurt Keutzer, et al. Sparsevlm: Visual token sparsification for efficient vision-language model inference. *arXiv preprint arXiv:2410.04417*, 2024.

[55] Qingqing Zhao, Yao Lu, Moo Jin Kim, Zipeng Fu, Zhuoyang Zhang, Yecheng Wu, Zhaoshuo Li, Qianli Ma, Song Han, Chelsea Finn, et al. Cot-vla: Visual chain-of-thought reasoning for vision-language-action models. In *Proceedings of the Computer Vision and Pattern Recognition Conference*, pp. 1702–1713, 2025.

[56] Ruijie Zheng, Yongyuan Liang, Shuaiyi Huang, Jianfeng Gao, Hal Daumé III, Andrey Kolobov, Furong Huang, and Jianwei Yang. Tracevla: Visual trace prompting enhances spatial-temporal awareness for generalist robotic policies. In *The Thirteenth International Conference on Learning Representations*, 2025.

[57] Brianna Zitkovich, Tianhe Yu, Sichun Xu, Peng Xu, Ted Xiao, Fei Xia, Jialin Wu, Paul Wohlhart, Stefan Welker, Ayzaan Wahid, et al. Rt-2: Vision-language-action models transfer web knowledge to robotic control. In *Conference on Robot Learning*, pp. 2165–2183. PMLR, 2023.

## Appendix

### A Implementation Details

We report the implementation details of our proposed AVA-VLA framework based on the OpenVLA-OFT architecture, and the training details of all experiments.

**Base OpenVLA-OFT architecture.** Our main experiments are based on the OpenVLA-OFT architecture. It integrates a shard SigLIP-DINOv2 backbone for multi-image processing, a Llama-2 7B language model, a 3-layer MLP projector with GELU activation for mapping visual features into the language embedding space, a 2-layer MLP with GELU activation for projecting robot proprioceptive state to the language embedding space, and a 4-layer MLP with ReLU activation for continuous action generation. Distinct from the standard OpenVLA, this architecture replaces causal attention with bidirectional attention to enable parallel decoding, outputting chunks of  $L_c$  actions at each timestep.

**AVA-VLA framework modifications.** Our main experiments introduce the following modifications for deploying the AVA-VLA framework on the OpenVLA-OFT foundation model: 1) a 2-layer MLP with SiLU activation for mapping hidden state to the forementioned recurrent state, 2) three 2-layer MLP with SiLU activation for mapping visual features, instruction feature, and recurrent state from  $d$ -dimension to  $d'$ -dimension, respectively, 3) a feature-wise linear modulation (FiLM) to condition the visual features on the language instruction, 4) a cross-attention layer, a self-attention layer, a FFN, and a linear layer with Softmax activation for predicting the logits for enhancing or weakening each vision token, 5) replaces the empty placeholder embedding with the recurrent state, 6) modifies the final attention weight matrix based on calculated soft weights vector from the AVA module.

**Training Details.** For the experiments on the LIBERO benchmark, we use their corresponding official OpenVLA-OFT checkpoints. To fine-tune the AVA-VLA model, we apply LoRA [12] with a rank of 32 to the LLM backbone, vision encoder, action head and proprioceptive projector, while fully optimizing the proposed AVA mechanism. We set the observation sequence length  $K = 4$ . For efficient training, the gradient is detached between the second and the third timestep. Hyperparameters are set as follows:  $\lambda = 1.0$ ,  $c = 0.6$ ,  $\gamma = [1.9, 0.1]$ . The action chunk size is set to  $L_c = 8$ . The batch size is set to 64. The model is trained for 40,000 gradient steps with an initial learning rate of 5e-4, which includes a warm-up phase by 10% of the value for stability. Additionally, a cosine learning rate scheduler and a maximum gradient norm of 1.0 is used. For the ablation study on the model backbone in Section 4.3, OpenVLA-OFT models follow standard implementation details [18] with varying initializations, and the AVA-VLA models are trained with implementation details described above using the corresponding OpenVLA-OFT models as initialization.

For the CALVIN benchmark, we train the base OpenVLA-OFT architecture following standard settings in [18] using official checkpoints. The AVA-VLA model is trained using the same configuration as the LIBERO benchmark, with the exception of setting  $c = 0.2$  to account for the smaller region of interest.

For Mobile ALOHA real-world experiments, inputs include one third-person and two wrist-mounted camera images (left wrist + right wrist), we provide the implementation details of the three comparison methods. For the UniVLA baseline, following [5], we fine-tune the pre-trained checkpoint using the recommended configuration. We employ the latent action decoder on primary images to obtain latent action supervision. We incorporate proprioceptive states into the action head and integrate dual wrist camera feeds as additional LLM inputs. The action chunk size is set to 25. The model is fine-tuned for 30,000 steps with a learning rate of 3.5e-4, which is decayed to 3.5e-5 after 24,000 steps. For the OpenVLA-OFT baseline, following [18], we use the official OpenVLA checkpoints as initialization, and apply the LoRA technique with a rank of 32 to the vision encoder and LLM backbone, while the action head and proprioceptive projector are fully optimized. The action chunk size is set to  $L_c = 25$ . The model is trained for 100,000 gradient steps with an initial learning rate of 5e-4. The learning rate is decayed to 5e-5 after 50,000 steps. The batch size is set to 64. For the AVA-VLA model, we utilize the trained OpenVLA-OFT model as initialization, and train the model for 20,000 gradient steps following our LIBERO hyperparameter settings, maintaining an action chunk size of  $L_c = 25$ .

### B Real-World Experiment Details

In this section, we report the additional details of the Mobile ALOHA real-world experiments, including the task suites and execution trajectories. We adopt AgileX Cobot Magic platforms: Based on Stanford’s Mobile ALOHA project<sup>2</sup>, this platform includes a differential-drive AGV base Tracer, dual-arm manipulators, and RGB-D sensors.

<sup>2</sup><https://global.agilex.ai/products/cobot-magic>

Table 6: Model performance under different perturbations in the LIBERO+ benchmark. For each column, the average task success rate (%) of four task suites (LIBERO-Spatial, LIBERO-Object, LIBERO-Goal, and LIBERO-Long) under the given perturbation type is reported. The last column reports the average task success rate over seven perturbation types. The best results in each column of each group are highlighted in **bold**.

	Camera	Robot	Language	Light	Background	Noise	Layout	Average
<i>One policy for all 4 suites</i>								
WorldVLA [6]	0.1	<b>27.9</b>	41.6	43.7	17.1	10.9	38.0	25.0
$\pi_0$ [3]	13.8	6.0	58.8	85.0	81.4	<b>79.0</b>	68.9	53.6
$\pi_0$ -FAST [32]	<b>65.1</b>	21.6	61.0	73.2	73.2	74.4	68.8	61.6
OpenVLA-OFT [18]	55.6	21.7	81.0	92.7	<b>91.0</b>	78.6	68.7	67.9
AVA-VLA (Ours)	55.5	25.9	<b>85.6</b>	<b>95.5</b>	88.9	78.0	<b>74.1</b>	<b>70.1</b>
<i>One policy per suite</i>								
OpenVLA [17]	0.8	3.5	23.0	8.1	34.8	15.2	28.5	15.6
NORA [13]	2.2	37.0	65.1	45.7	58.6	12.8	62.1	39.0
UniVLA [5]	1.8	<b>46.2</b>	69.6	69.0	81.0	21.2	31.9	42.9
OpenVLA-OFT [18]	56.4	31.9	79.5	88.7	93.3	75.8	74.2	69.6
RIPT-VLA [42]	55.2	31.2	77.6	88.4	91.6	73.5	74.2	68.4
AVA-VLA (Ours)	<b>69.4</b>	34.9	<b>81.5</b>	<b>97.5</b>	<b>94.1</b>	<b>79.1</b>	<b>78.3</b>	<b>74.7</b>

## B.1 Real-World Task Suites

We introduce the detailed specifications for each task suite in our Mobile ALOHA real-world experiments:

### Pick and Place

- Instructions: “put X into bucket”.
- Task: Place the bucket in the center and put the simulated toy objects of which the instruction has given (yellow banana, green pepper, purple eggplant) into the bucket.
- Dataset: 450 demonstrations (150 per target).
- Episode length: 700 timesteps (28 seconds).
- Evaluation: 30 trials (10 for each).

### Sequenced Instruction Understanding

- Instruction: “stack tower of hanoi”.
- Task: Stack the medium tower on top of the large one first, and then stack the small one on top of the medium one.
- Dataset: 60 demonstrations (10 per formulation).
- Episode length: 600 timesteps (24 seconds).
- Evaluation: 24 trials (4 for each).

### Flexible Object Folding

- Instruction: “fold towel twice”.
- Task: First fold the towel vertically, then fold horizontally, and finally flatten it.
- Dataset: 30 demonstrations.
- Episode length: 900 timesteps (36 seconds).
- Evaluation: 24 trials.

### Dexterous Action

- Instructions: “scoop X into bowl”.
- Task: Move the bowl to the center of vision, pick up and use the shovel to scoop up different objects (corn, sesame, sunflower seeds) and transfer them into the bowl.
- Dataset: 60 demonstrations (20 of each small object).
- Episode length: 1000 timesteps (40 seconds).
- Evaluation: 24 trials (8 for each).

## C Additional Experimental Results

In this section, we report the additional experimental results, including the additional results on the LIBERO+ Benchmark and additional qualitative visualization results.

### C.1 Additional Results on LIBERO+ Benchmark

The LIBERO+ [11] benchmark enables us to perform a systematic vulnerability analysis by introducing controlled perturbations across seven dimensions: camera viewpoints (change the viewpoint/pose and field-of-view of the third-person camera), robot initial states (change the manipulator’s initial pose), language instructions (rewrite task instructions to increase linguistic richness and complexity), light conditions (vary illumination intensity, direction, color, and shadow patterns), background textures (modify table/scene textures and materials), sensor noise (inject photometric distortions into input images), and object layout (add confounding objects and/or shift the target object’s position).

We evaluate the proposed method on the LIBERO+ benchmark using the AVA-VLA models trained on the LIBERO benchmark. We do not use additional data to train these models. The evaluation results of two different settings: “one policy for all 4 suites” and “one policy per suite” are reported in Table 6. The results of baselines in LIBERO+ benchmarks are based on original references [11]. The results show that the proposed AVA-VLA method achieves the best total results over the seven perturbation types on two different settings, demonstrating the superiority of the proposed framework. Notably, the AVA-VLA model exhibits strong robustness under the Light and the Layout perturbations, further demonstrating that the proposed AVA module helps the model enhance the important visual information and reduce the interference of unimportant parts on prediction, thereby improving the model’s robustness under visual interference.

### C.2 Additional Results on Qualitative Visualization

In Section 4.4, we visualize the soft weights  $\omega^t$  related to the corresponding visual tokens during the inference of one example from the LIBERO benchmark. Additionally, we present further visualizations of the soft weights calculated by the AVA module across a broader set of examples to demonstrate the proposed method’s consistency.

Figure 6 and Figure 7 illustrate results from Mobile ALOHA real-world experiments, covering two task suites across three viewpoints. The results demonstrate the proposed framework’s ability to focus on important visual information. Specifically, in the “put yellow banana into bucket” task, the model consistently locates and focuses on the objects requiring interaction: the yellow banana and the bucket. Similarly, for the “scoop sesame into bowl” task, the model accurately pinpoints the interaction target, such as the ladle handle in frame 375 of the right wrist-mounted camera.

Extended visualization results for simulated environments are presented in Figures 8, 9, and 10. Figure 8 displays the results for the continuous tasks “Lift red block table” and “Place in slider” from two viewpoints for the experiment on the CALVIN benchmark. Figure 9 and Figure 10 display the results for two tasks from two viewpoints for the experiment on the LIBERO benchmark, respectively. These additional visualization results on the simulation environments consistently corroborate our findings. The proposed AVA-VLA method can enable the VLA model to effectively enhance the perception of critical visual information while suppressing irrelevant regions, thereby improving the model’s performance.

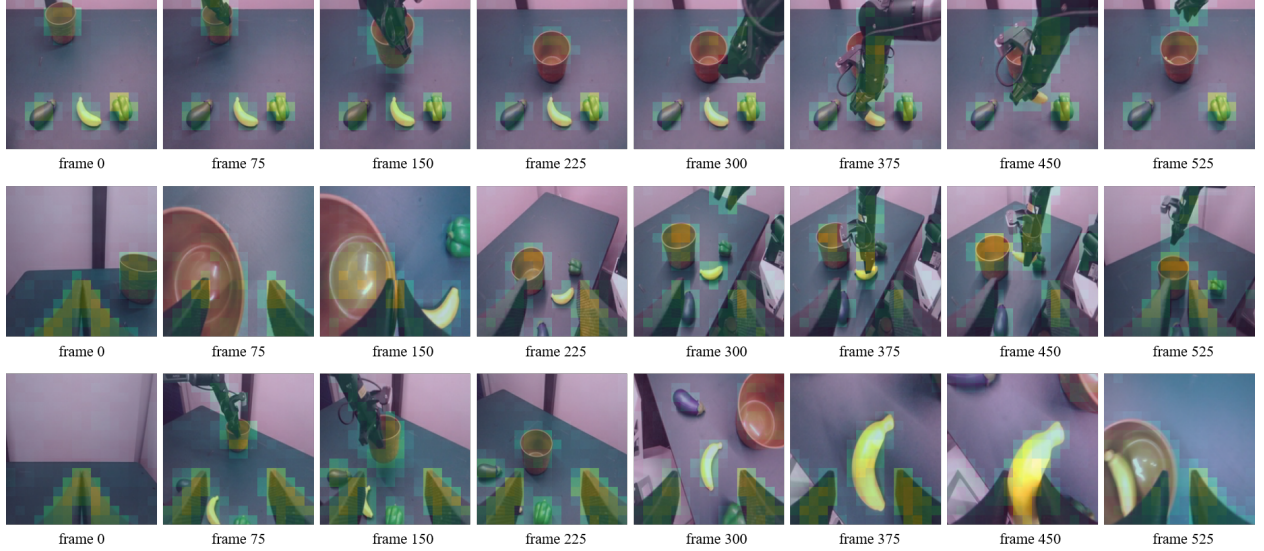


Figure 6: Visual dynamics of the soft weights during the task “put yellow banana into bucket” in three viewpoints for Mobile ALOHA real-world experiments.

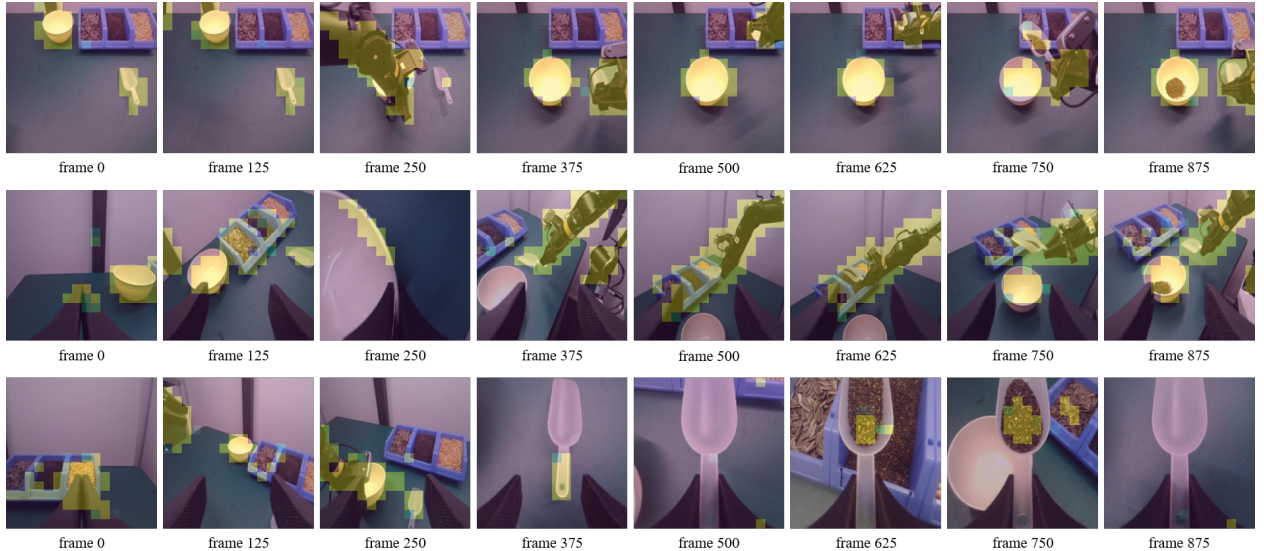


Figure 7: Visual dynamics of the soft weights during the task “scoop sesame into bowl” in three viewpoints for Mobile ALOHA real-world experiments.

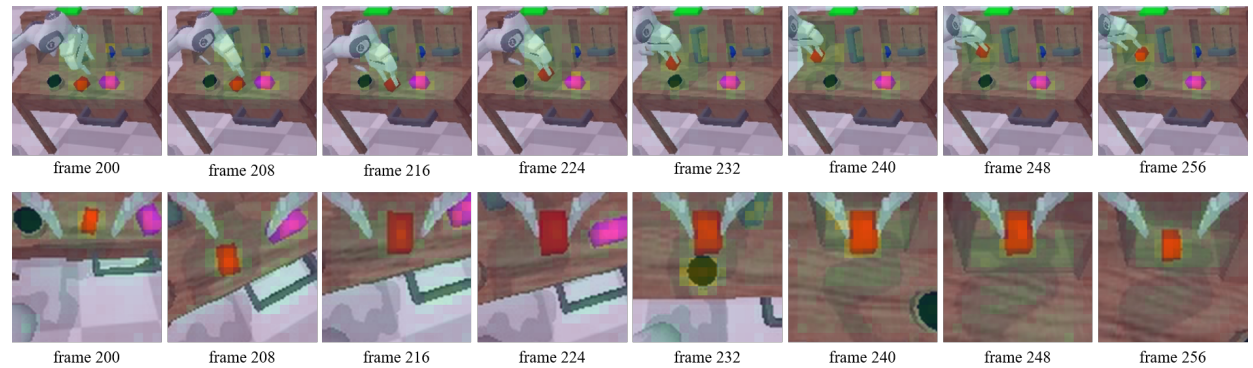


Figure 8: Visual dynamics of the soft weights during the continuous tasks “Lift red block table” and “Place in slider” in two viewpoints for the experiment on the CALVIN benchmark.

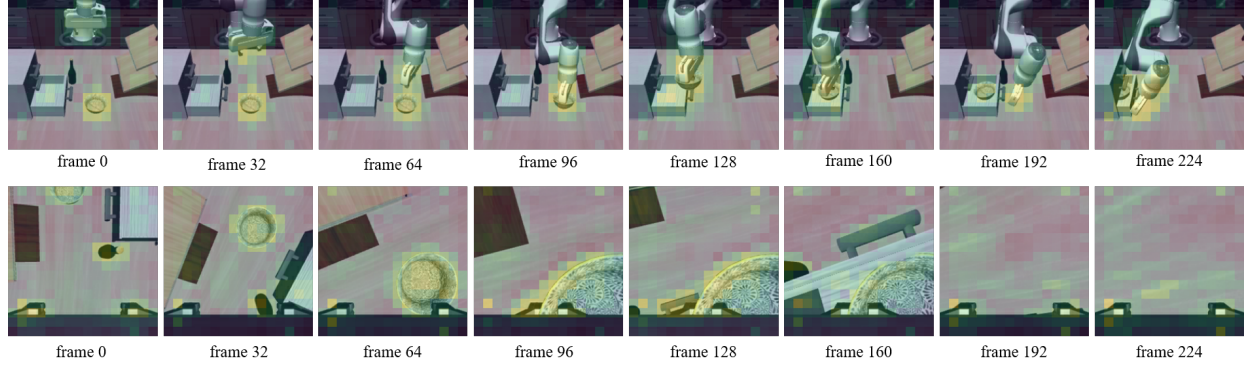


Figure 9: Visual dynamics of the soft weights during the task “put the black bowl in the bottom drawer of the cabinet and close it” in two viewpoints for the LIBERO benchmark.

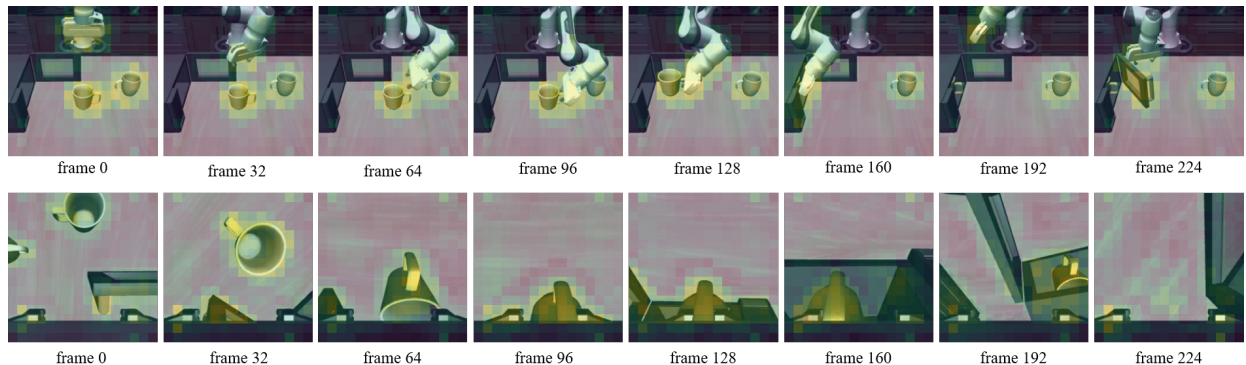


Figure 10: Visual dynamics of the soft weights during the task “put the yellow and white mug in the microwave and close it” in two viewpoints for the LIBERO benchmark.